J. Wind Eng. Ind. Aerodyn. 99 (2011) 414–423

Contents lists available at ScienceDirect

Journal of Wind Engineering and Industrial Aerodynamics

journal homepage: www.elsevier.com/locate/jweia

Evaluation of the ventilation potential of courtyards and urban street canyons using RANS and LES

P. Moonen [a,b,*], V. Dorer [b], J. Carmeliet [a,b]

[a] ETH, Swiss Federal Institute of Technology Zürich, Zürich, Switzerland
[b] Empa, Swiss Federal Laboratories for Materials Science and Technology, Überlandstrasse 129, 8600 Dübendorf, Switzerland

ARTICLE INFO

Available online 28 January 2011

Keywords:
Ventilation potential
Computational fluid dynamics (CFD)
Reynolds-averaged Navier–Stokes (RANS)
Large eddy simulation (LES)
Courtyard
Street canyon
Ambient wind direction
Oblique flow

ABSTRACT

We introduce the ventilation potential (VP) as a statistical, climate-dependent measure to assess the removal of scalars, such as heat and pollutants, from courtyards or urban street canyons. The VP is obtained following a three-step approach. First, the magnitude of the flux through a horizontal surface situated at the top of the courtyard or canyon is determined by means of computational fluid dynamics (CFD) simulations for various courtyard geometries and ambient wind directions. Then, this exchange flux is normalized with the free-stream wind speed and subsequently parameterized as a function of the courtyard's length-to-width ratio and the incidence angle of the wind flow. Finally, the combination of the parameterization with site-specific wind data yields the VP. This study reveals that the normalized exchange flux is maximal when the angle between the prevailing flow direction and the main courtyard axis is about 15–30°, regardless of the courtyard length. The normalized exchange flux increases with increasing courtyard length, and approaches the optimum for courtyards with a length-to-height ratio of ten. Longer courtyards behave as urban street canyons. Unsteady (LES) simulations lead to a much higher VP and thus favor scalar removal when compared with steady (RANS) simulations. These observations can have a decisive impact on urban planning, human comfort and health.

1. Introduction

Vehicular emission is one of the major sources of anthropogenic pollutants in urbanized cities (Liu et al., 2005). The majority of these emissions occur in the urban street canyon. Because of their adverse impact on human health, numerous studies have been conducted to enrich our understanding of scalar removal mechanisms in urban street canyons. Wind tunnel measurements were performed on isolated street canyons without (e.g. Pavageau and Schatzmann, 1999) and with trees (e.g. Gromke and Ruck, 2009), on arrays of street canyons (e.g. Sagrado et al., 2002), on street intersections (e.g. Soulhac et al., 2009) and on urban models (e.g. Pascheke et al., 2008). Computational fluid dynamics (CFD) has been used to study street canyons of different aspect ratio's (Sini et al., 1996), regular arrays of building blocks (e.g. Martilli and Santiago, 2007) and urban configurations (e.g. Tominaga et al., 2004).

Despite the vast amount of research conducted to date, studies on the effect of the ambient wind direction on the air exchange and scalar removal mechanisms in courtyards or street canyons are scarce. The few available studies (Kim and Baik, 2004; Ryu and Baik, 2009) indicate that the ambient wind direction can greatly affect the characteristics of flow and dispersion. Field measurements confirm that knowledge on the relative geometry of the canyon itself is therefore no longer sufficient to determine the fundamental nature of the flow (Johnson and Hunter, 1999).

In this paper, we numerically investigate the effect of the ambient wind direction on the ventilation performance of idealized courtyards, characterized by five different length-to-width ratios. Since previous studies (Baik and Kim, 2002; Liu et al., 2005; Cheng et al., 2008) pointed out the importance of turbulent fluctuations on pollutant removal processes, both steady and unsteady numerical simulations are conducted and mutually compared. The paper is structured in four main parts. Section 2 provides a detailed description about many aspects of the computational model. Section 3 presents the results of the steady and unsteady CFD simulations for the idealized courtyards. The main quantity of interest is the amount of air exchange between the courtyard and the air flow above. The exchange flux proved to depend on the length-to-width ratio of the courtyard and the ambient wind direction. Marked differences between steady and

* Correspondence to: Empa, Swiss Federal Laboratories for Materials Science and Technology, Überlandstrasse 129, 8600 Dübendorf, Switzerland
E-mail addresses: moonen@arch.ethz.ch, peter.moonen@empa.ch (P. Moonen), viktor.dorer@empa.ch (V. Dorer), carmeliet@arch.ethz.ch, jan.carmeliet@empa.ch (J. Carmeliet).

0167-6105/$ - see front matter © 2011 Published by Elsevier Ltd.
doi:10.1016/j.jweia.2010.12.012

unsteady simulations are observed. In Section 4, the exchange flux is parameterized as function of the dominant factors. Because a street canyon can be considered as the limit case of a courtyard with an infinite length-to-width ratio, its exchange rate is obtained by extrapolating the proposed parameterization. Finally, the term ventilation potential (VP) is introduced in Section 5. This quantity provides a statistical, climate-dependent measure of the removal of scalars from the courtyard or urban street canyon. The VP has a different purpose than other recently introduced indices for outdoor air exchange and pollutant removal in urban areas (e.g. Bady et al., 2008; Buccolieri et al., 2010; Hang et al., 2009; Kato and Huang, 2009), which have been developed by transferring concepts originally deployed for the characterization of ventilation and pollutant removal performance in indoor spaces. Such indices quantify the air quality in an urban area under given climatic conditions, while the VP gives insight in the effect of local wind conditions, such as the distribution of wind speed and direction, on the exchange rate, and hence the air quality.

2. Computational model

2.1. Domain dimensions

We study isolated elongated courtyards with a cross section of 16×16 m^2 ($w \times h$) and a length ℓ. Five different lengths (1, 2, 5, 10 and 20 times the courtyard height h) are considered in this study. Each courtyard is submersed in a large flat plate, representing the upper edge of the urban domain, as illustrated in the inset of Fig. 1. The courtyard walls are assumed to be smooth, and the courtyard itself is free of obstructions such as trees or cars. Although important, interaction between different courtyards is not considered in this study.

A hexahedral computational domain is used (Fig. 1). Bechmann (2006) conducted channel flow simulations by means of large eddy simulation (LES) and found that the largest scales of motion are unrestricted if the domain width W exceeds 3.5 times the domain height H. He recommends a domain length L of 6 times the domain height in order to avoid the presence of marked peaks at frequencies corresponding to multiples of the domain length in case periodic boundary conditions are imposed. Following Bechmann (2006), we use a domain with proportions 3.5:1:6 (W/H:H/H:L/H, see Fig. 1). A domain height of 128 m ($8h$) is selected, representing the lower part of the atmospheric boundary layer (ABL).

The courtyard is positioned at $8h$ from the upstream domain boundaries (denoted side 1 and 2 in Fig. 1). For the longest courtyard ($\ell = 20h$), the downstream domain boundaries are situated at $20h$ (denoted side 3 and 4 in Fig. 1). Both upstream and downstream distances are large compared to typical domain sizes employed when studying isolated buildings (Franke et al., 2007).

2.2. Boundary conditions

We simulate the flow in the surface layer of a neutral atmospheric boundary layer, in absence of temperature effects. Thermal stratification, although important, has not been considered in this study. Boundary conditions (BCs) are chosen as follows.

At the *top boundary* of the domain, symmetry is imposed. This type of BC suppresses the fluctuations normal to the boundary and enhances the in-plane fluctuations. Given the large height of the computational domain as compared to the courtyard depth, this is expected to have a negligible influence on the air flow pattern in the courtyard.

At the *bottom boundary* of the domain, a no-slip wall BC is imposed, corresponding to flow over smooth terrain. The same type of BC is imposed to the courtyard walls. This choice allows comparing steady Reynolds-averaged Navier–Stokes (RANS) simulations to unsteady simulations with LES, in which roughness would need to be explicitly modeled. The latter is a restriction of the employed software package (Ansys Fluent 12.0).

Three types of *lateral boundaries* are used in the simulations, namely inflow, outflow and periodic boundaries. On inflow boundaries, profiles for velocities and, in the case of RANS, for turbulent kinetic energy and energy dissipation are specified. These mean profiles are obtained from a precursor simulation, as will be explained in Section 3.1, and are depicted in Fig. 2. For LES, time-dependent inlet conditions are generated from the mean profiles using the vortex method (Sergent, 2002). For outflow boundaries, a zero static back-pressure is assumed. Periodic boundaries imply that certain flow quantities repeat themselves in space.

The total range of possible wind directions is subdivided into 24 sectors of 15°. Because of the planes of symmetry of the courtyard, simulations can be reduced to seven incident flow directions, namely 0° (wind flow parallel to the principal courtyard axis), 90° (wind flow orthogonal to the principal courtyard axis) and five intermediate directions (15°, 30°, 45°, 60° and 75°). For the 0°-case, side 1 is an inflow boundary, side 3 is the outflow boundary and sides 2 and 4 are considered periodic. For the 90°-case, sides 2 and 4 are the in- and outflow boundaries, respectively, while sides 1 and 3 are periodic. For the five remaining cases, sides 1 and 2 are both inflow boundaries, while sides 3 and 4 are outflow boundaries.

2.3. Computational grid

One of the goals of this study is to assess the impact of turbulent structures on scalar removal processes. Therefore,

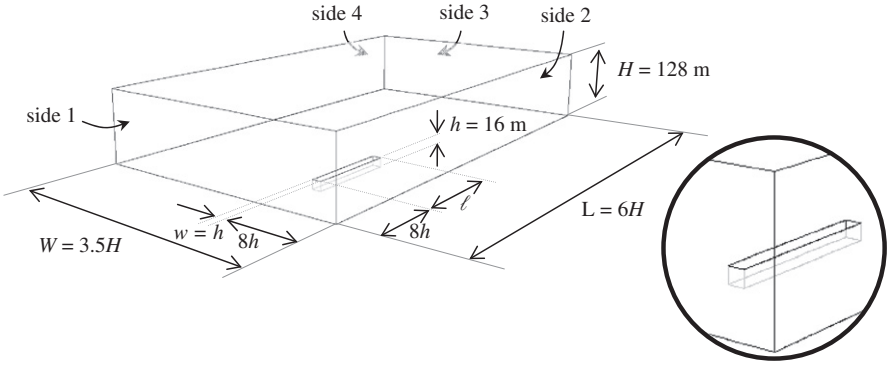

Fig. 1. Layout of the computational domain with courtyard.

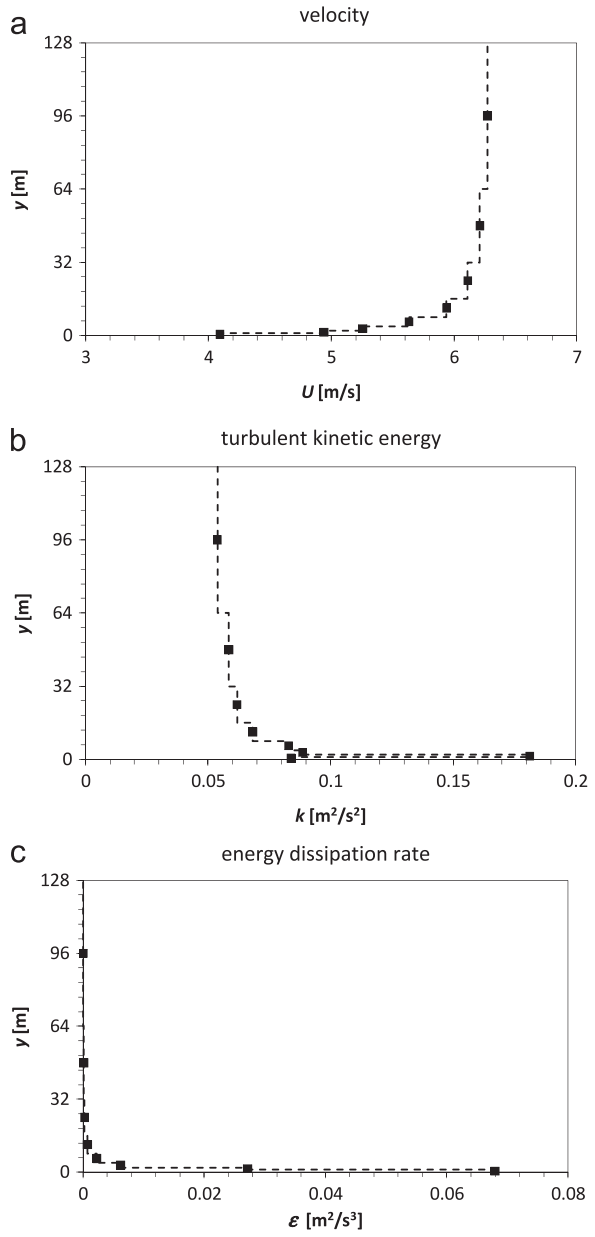

Fig. 2. Vertical profiles for (a) velocity, (b) turbulent kinetic energy and (c) energy dissipation rate. The markers indicate cell values; the dashed line represents the profile if constant values are assumed within a computational cell.

steady RANS simulations, in which all turbulent length scales are modeled, are compared to unsteady LES computations, in which only the small turbulent length scales are modeled. Hereby, the computational grid acts as a filter, and only the turbulent structures larger than the grid size are solved. Cubic elements have an equal filter length in the three principal directions, and are therefore the most optimal element type for resolving turbulent structures.

The meshes employed in this study consist of 802.788 cubic elements (for the precursor simulation, i.e. without courtyard), up to 884.708 cubic elements (for the mesh with the longest courtyard). The smallest elements ($1 \times 1 \times 1$ m^3) are located near the ground and inside the courtyard. The mesh size gradually increases towards the top of the domain. The largest elements measure $64 \times 64 \times 64$ m^3. The employed cell sizes in the region of interest (i.e. the courtyard) are about 40% more refined than the recommended grid sizes for isolated buildings (Franke et al., 2007) and for idealized street canyons (Bartzis et al., 2004).

2.4. Solution method

The three-dimensional Navier–Stokes equations and the continuity equation were solved using the commercial CFD code Ansys Fluent 12.0 that employs the control-volume technique. The staggered pressure-based solver was selected.

For the steady RANS simulations, closure was obtained by using a realizable k–ε turbulence model (Shih et al., 1995). Near-wall modeling was performed using non-equilibrium wall functions (Kim and Choudhury, 1995). Pressure–velocity coupling was taken care of by the SIMPLEC algorithm (Vandoormaal and Raithby, 1984). Second-order pressure interpolation was used. The third-order MUSCL discretization scheme (Van Leer, 1979) was used for the convection terms of the governing equations and the equations of the turbulence model.

For the unsteady LES simulations, closure was obtained by means of the dynamic Smagorinsky–Lilly subgrid-scale model (Lilly, 1992). Pressure–velocity coupling was taken care of by the SIMPLEC algorithm (Vandoormaal and Raithby, 1984). Second-order pressure interpolation was used. The second-order accurate bounded central differencing scheme is used for the momentum equations. Green–Gauss node-based gradient evaluation is employed.

Calculations were run until the desired level of convergence was reached, i.e. constant residuals of 10^{-4} or less for all equations (Franke et al., 2007). The residuals are defined as the imbalance of the conservation equations, summed over all elements. These values are scaled and the scaled values are used in the code as a measure of the iteration convergence (Ansys Inc., 2009).

2.5. Initialization and computation

The RANS simulations were initialized with a uniform field for velocity (5 m/s in the desired flow direction), turbulent kinetic energy (0.05 m^2/s^2) and energy dissipation rate (0.005 m^2/s^3). Typically 3000 iterations were required to reach convergence.

The LES solution was initialized from the fully converged RANS solution. A time step of 1 s was selected, resulting in average Courant numbers below 5. Typically 100 iterations were required per time step. Preliminary studies showed that a stable flow pattern is reached after 100 s. Calculations were run for a period of 300 s, corresponding to more than two domain flow-through times. Only the last 200 s were used for data processing.

3. Results and discussion

3.1. Precursor simulation

Richards and Hoxey (1993) derived formulae for the vertical profiles of velocity (u), turbulent kinetic energy (k) and energy dissipation rate (ε) in a homogeneous ABL, which are widely used as inlet conditions for CFD simulations. Nevertheless, these velocity and turbulence profiles were found to decay with distance, even in the absence of obstructions, due to incompatibility with the employed law-of-the-wall. Horizontal homogeneity can be obtained by modifying the law-of-the-wall (e.g. Blocken et al., 2007; Hargreaves and Wright, 2007), or, by determining suitable vertical profiles from a precursor simulation. The latter approach is more straightforward when different modeling approaches are compared, and is employed here.

Our precursor simulation is a steady RANS simulation that employs the same combination of numerical models and discretization schemes as the actual simulations. The domain is identical to the one described in Section 2.1, but in absence of the courtyard. All four lateral boundaries are considered (translationally) periodic. A pressure difference of 0.2 Pa is imposed between boundaries 1 and 3 (see Fig. 1) to drive the flow. The resulting profiles (Fig. 2) are in mutual equilibrium for the given computational setup and are exactly preserved along the entire domain. Identical profiles develop for the other six wind directions, demonstrating the limited amount of numerical diffusion for the combination of numerical schemes (Section 2.4) employed in this study.

3.2. Wind flow pattern in a 1:1:1 courtyard

First, we study the wind flow pattern in the 1:1:1 courtyard (w/h:h/h:ℓ/h, with $h=16$ m) for various wind directions. We focus on the total upward flux through two horizontal planes, one situated at the top of the courtyard, and one at half of the courtyard height (Fig. 3(a)). The upward flux is defined as

$$f_S = \int_S \frac{v+|v|}{2} dS \tag{1}$$

for RANS and

$$f_S = \frac{1}{200}\int_{100}^{300}\int_S \frac{v+|v|}{2} dS dt \tag{2}$$

for LES, with v the vertical velocity component, $|\cdot|$ the absolute value operator, S the surface under study (i.e. "top" or "mid") and t the time (ranging from $t=100$ to $t=300$ s). In the remainder, the total upward flux through the top plane (f_{top}) is also referred to as the exchange flux between the courtyard and the urban boundary layer. The applied convention related to the wind direction is indicated in Fig. 3(b).

Fig. 4(a) plots the magnitude of the total upward flux through the top and mid-plane as a function of the incident flow direction, as obtained from steady RANS simulations. Two interesting observations can be made. (i) The upward flux through the mid-plane is about ten times larger than the upward flux through the top-plane, regardless of the flow direction. (ii) The maximum exchange flux takes place at an incidence angle of $\pm(30°+n90°)$ with n an integer number.

The first observation indicates the presence of a standing vortex in the courtyard, quasi-uncoupled from the skimming flow in the urban boundary layer. Fig. 4(b) depicts the typical air flow pattern for the $0°+n90°$ incidence angles. It is clear that passive scalars, when released in the courtyard, will have a very long residence time, i.e. they are "trapped".

If the incident wind flow is oblique to the planes of symmetry of the courtyard, a more complex flow pattern arises, leading to a higher exchange flux through the top-plane. The maximum exchange flux (12.2 m^3/s) is observed at an incidence angle of $\pm(30°+n90°)$. The lowest exchange flux (3.4 m^3/s), occurring for across-courtyard flow ($0°+n90°$), is about 3.5 times smaller.

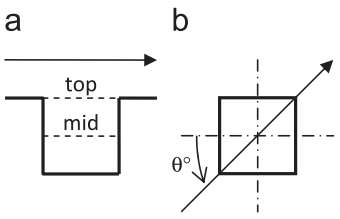

Fig. 3. (a) Position of the investigated planes relative to the courtyard (side view). (b) Convention related to wind direction (top view).

The magnitude of the total upward flux through the top and mid-plane has been studied by means of LES as well. In Fig. 5, the time-averaged LES results (solid lines) are compared to the steady RANS results (dashed lines). The LES simulations support the main observations that (i) the flux through the mid-plane is larger than the flux through the top-plane, regardless of the flow direction (please note the difference of scale between Fig. 5(a) and (b)) and (ii) wind flow with an incidence angle of $\pm(30°+n90°)$ leads to the maximum exchange flux between the courtyard and the air flow in the urban boundary layer. Nevertheless, the angular dependency of the time-averaged exchange flux through the top surface is much less pronounced than the corresponding variation found in the RANS-based simulations (Fig. 5(a)). The angular dependency of the flux through the mid-plane shows the same trend for RANS and LES, although the LES values are 20–30% lower (Fig. 5(b)).

Comparing Fig. 5(a) and (b), it is clear that the steady RANS results predict a strong correlation between the magnitudes of the upward fluxes through top and mid-plane for every wind direction. In fact, the ratio between both is always $\approx 10\%$, regardless of the incidence angle of the wind flow (Fig. 6(a), dashed line). The unsteady LES simulations also show some correlation – higher fluxes through the top plane go with higher fluxes through the mid-plane and vice versa – but the correlation is clearly weaker (Fig. 6(a), solid line). This is believed to be due to the unsteady character of the flow, which is partially resolved in the LES, and fully modeled in the RANS simulations. Nevertheless, other factors, like the values of the parameters in the turbulence model (RANS) and the subgrid-scale model (LES), might also have an effect on the obtained flow pattern and the resulting fluxes through the top and mid-plane.

3.3. Wind flow pattern in elongated courtyards

Additional simulations were performed for courtyards with a length ℓ of 2, 5, 10 and 20 times the courtyard height h, both with RANS and LES. The same 7 wind directions were studied.

Fig. 7 shows the ratio between the total upward flux through the top and mid-plane for the four elongated courtyard configurations as a function of the ambient wind direction. For comparison, the top-to-mid ratio for the cubic 1:1:1 courtyard is presented in Fig. 6(a). The RANS results are depicted with dashed lines, while the LES results are denoted with solid lines. Note that a logarithmic scale is used. Generally, it can be observed that the top-to-mid ratio increases with increasing courtyard length for along-courtyard flow ($0°+n180°$), but is hardly affected by the courtyard length for across-courtyard flow ($90°+n180°$). A higher top-to-mid ratio implies a stronger interaction between the fluxes above and in the courtyard. A ratio above one is found for the most elongated courtyards for incident wind flow within the interval $-15° \le \theta \le 15°$ (or $165° \le \theta \le 195°$). This reflects a change in the type of flow pattern. If the courtyard's length-to-height ratio is small ($\ell/h \le 5$), an isolated standing vortex is formed (Fig. 8(a)). For a high length-to-height ratio ($\ell/h \ge 10$), the flow submerses in the courtyard at one end, and surfaces at the other end (Fig. 8(b)). For intermediate ratios ($5 < \ell/h < 10$) a transition regime is found. These three regimes are comparable to the classification into isolated roughness, wake interference and skimming flow based on a street canyon's height-to-width ratio (Oke, 1988).

The largest differences between the top-to-mid ratios based (i) on steady RANS and (ii) on time-averaged LES data are found for the shortest courtyard and vanish with increasing courtyard length. In the case of the 1:1:1 courtyard, these differences were attributed to the flow unsteadiness (see Section 3.2). For very long

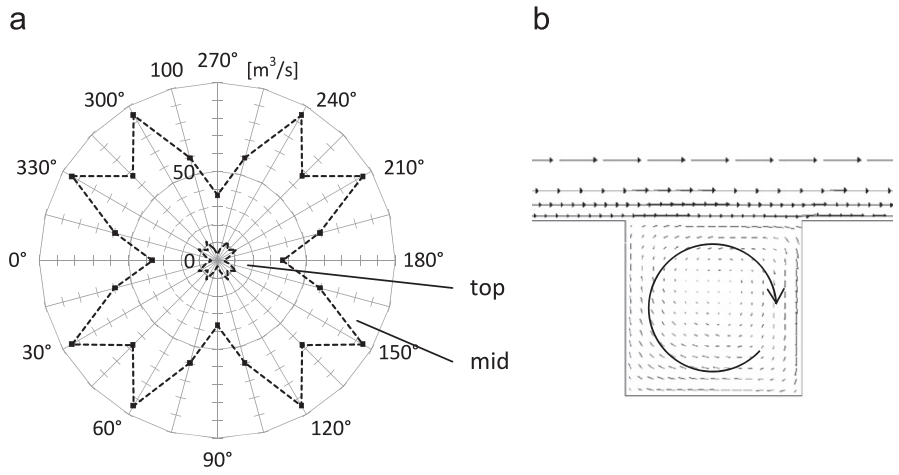

Fig. 4. (a) Magnitude of the total upward flux through the two horizontal planes as a function of the wind direction, as obtained via RANS. (b) Air flow pattern for the 0°, 90°, 180° and 270°-cases.

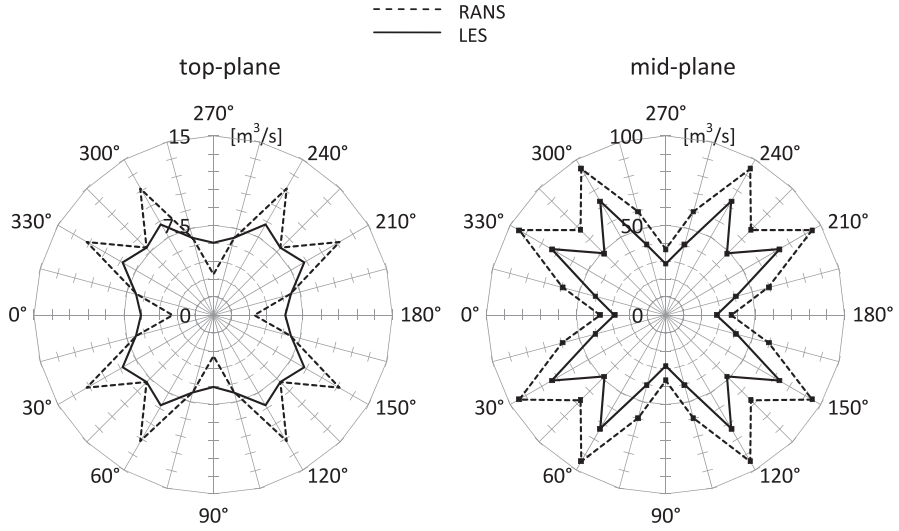

Fig. 5. Magnitude of the total upward flux through (a) the top-plane and (b) the mid-plane as a function of the wind direction. Dashed lines correspond to RANS simulations, solid lines to LES.

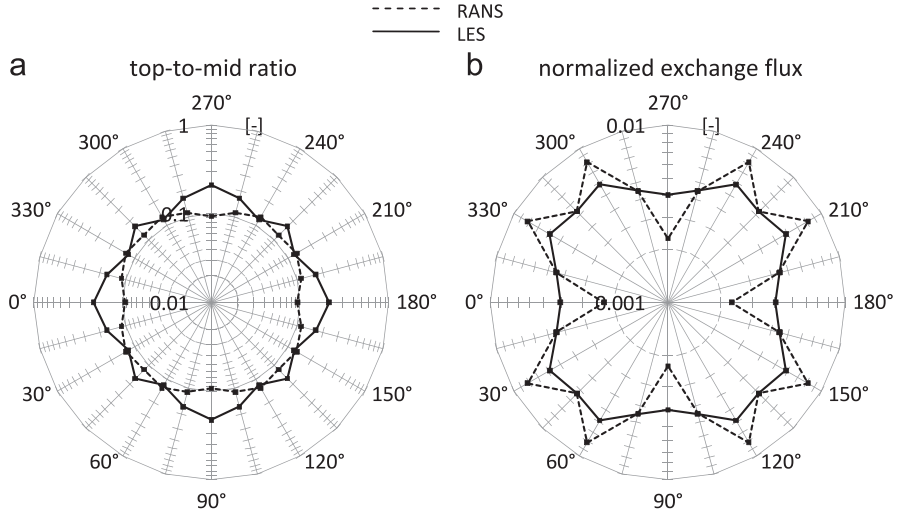

Fig. 6. (a) Ratio between the total upward flux through the top and mid-plane and (b) normalized exchange flux via the top-plane, as a function of wind direction for a 1:1:1 courtyard. Dashed lines correspond to RANS simulations, solid lines to LES.

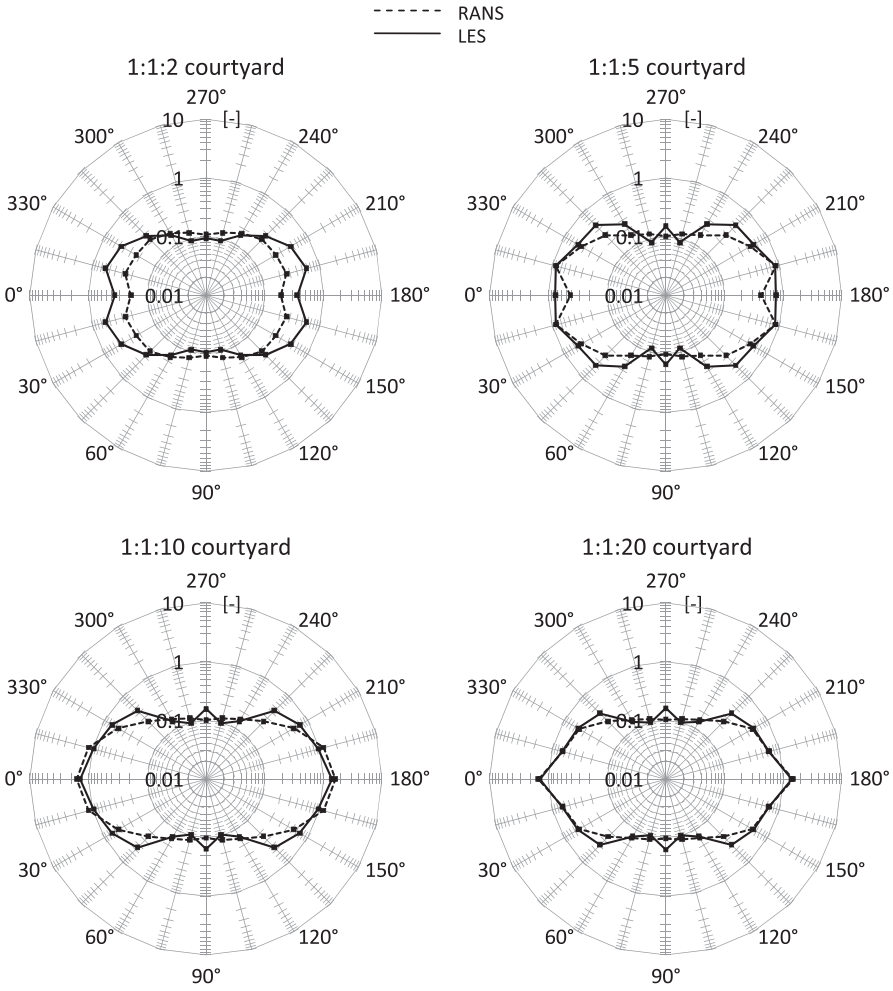

Fig. 7. Ratio between the total upward flux through the top and mid-plane as a function of wind direction and courtyard length for 4 courtyard ℓ/h ratios. Dashed lines correspond to RANS simulations, solid lines to LES.

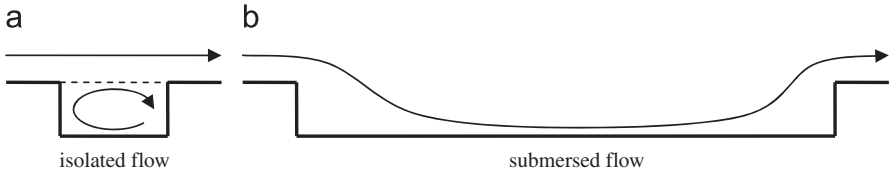

Fig. 8. Different flow patterns for (quasi) along-courtyard flow depending on the courtyard's ℓ/h ratio.

courtyards the temporal flow characteristics seem to have less importance, i.e. the structural flow behavior prevails over the local fluctuations.

We define the normalized exchange flux $f_{\ell,\theta}$ through the top-plane of a courtyard with length ℓ and width w as

$$f_{\ell,\theta} = \frac{f_{top}}{(\ell \times w) \times U_{10,\theta}} \tag{3}$$

where f_{top} is the total upward flow through the top-plane and $U_{10,\theta}$ is the (horizontal) reference wind speed at 10 m height (U_{10}=5.84 m/s, see Fig. 2(a)) coming from direction θ.

Fig. 9 depicts $f_{\ell,\theta}$ for the four elongated courtyard configurations as a function of the wind direction. For comparison, the normalized exchange flux for the cubic 1:1:1 courtyard is shown in Fig. 6(b). RANS results are depicted with dashed lines, while the LES results are denoted with solid lines. Note that a logarithmic scale is used. Generally higher normalized exchange fluxes are obtained with LES. The differences between RANS and LES tend to vanish with increasing courtyard length.

Similar to the top-to-mid ratio, $f_{\ell,\theta}$ is hardly affected by the courtyard length for across-courtyard flow ($90°+n180°$). This indicates (i) that the size of the standing vortex is primarily determined by the height-to-width ratio of the courtyard and (ii) that boundary effects at both ends of the courtyard do not play a significant role for this wind direction, even for the shortest courtyard.

For all other wind directions, $f_{\ell,\theta}$ tends to increase with increasing courtyard length. Increasing the courtyard length beyond 10h only has a minor effect on the normalized exchange flux, indicating that boundary effects are negligible. Courtyards with a length of 10h or more can therefore be considered as urban street canyons.

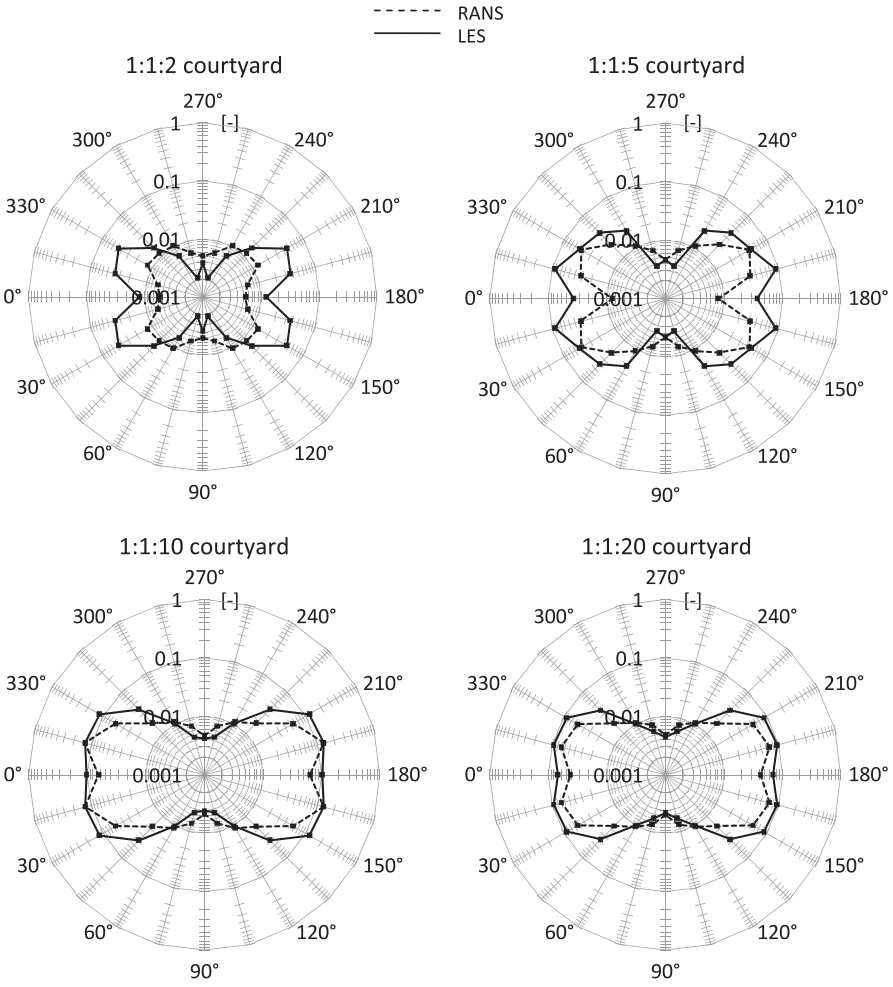

Fig. 9. Normalized exchange flux via the top-plane, as a function of wind direction and courtyard length for 4 courtyard configurations. Dashed lines correspond to RANS simulations, solid lines to LES.

The highest normalized exchange fluxes are observed for a 15–30° incidence angle. Under these conditions a helical vortex is formed within the elongated courtyard (Fig. 10).

4. Parameterization of the normalized exchange flux

In this section, a relation expressing the normalized exchange flux as a function of courtyard length and ambient wind direction is established. The purpose of proposing such relationship is twofold. On the one hand, it allows assessing the exchange flux of a courtyard with arbitrary length and width as a function of the wind direction, without relying on time and computationally intensive CFD calculations. On the other hand, such relation provides a simple means to study the exchange flux as a function of courtyard length for a given ambient wind direction. By systematically increasing the courtyard length to infinity, the behavior of the (infinite) street canyon under oblique approach flow conditions can be investigated.

The parameterization should comply with some geometrical constraints. For instance, an elongated courtyard has two vertical planes of symmetry. Therefore, flow from 30°, 150°, 210° and 330° should result in the same exchange flux. For a courtyard with $\ell = w$, two additional vertical planes of symmetry exist, and therefore wind flow from e.g. 30° and 60° is equivalent.

A second type of geometrical constraint is related to the courtyard geometry. In a courtyard with an elliptical ground surface, the (time-averaged) flow pattern would gradually change with varying incidence angle and the exchange fluxes as well. For courtyards with a quadrilateral ground surface, this is no longer true. Since the ground surface exhibits sharp corners, the corresponding incidence angles (i.e. when the approaching flow is aligned with the diagonal of the ground surface of the courtyard), can correspond to a sharp local peak (or dip) of the exchange fluxes. Such peaks can for example be observed in Fig. 9 at 30° for the 1:1:2 courtyard and around 15° for the 1:1:5 courtyard.

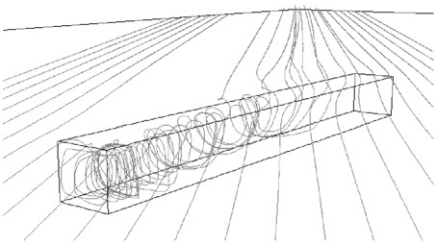

Fig. 10. Helical flow pattern for oblique incident wind flow (1:1:10 courtyard, RANS, 30°).

The expression for the normalized exchange fluxes should satisfy both types of geometrical constraint, and is therefore constructed on the basis of cosine functions with a period of $360°/(2n)$ for elongated courtyards, and with a period of $360°/(4m)$ for the 1:1:1 courtyard, with n and m integer numbers.

Note that the latter set of harmonics is a subset of the former one, obeying $n=2m$. Therefore, we can generally write

$$f_{\ell,\theta} = \left[\sum_n A_{2n}\cos(2n\theta_{eq})\right] + B_2[1-|\cos(2\theta_{eq})|] \quad (4)$$

where the last term is added to be able to capture the sharp local peak (or dip) when the wind flow aligns with the diagonal of the courtyard. Coefficients A_{2n} and B_2 are the amplitudes of the corresponding harmonic contributions. For reasons that will be explained below, these are formulated in terms of an equivalent angle θ_{eq}, a function of the wind direction θ. The more terms are considered in the summation, the more accurate Eq. (4) will be. We limit ourselves to the first 4 terms ($n=4$)

$$f_{\ell,\theta} = [A_0 + A_2\cos(2\theta_{eq}) + A_4\cos(4\theta_{eq}) + A_6\cos(6\theta_{eq}) + A_8\cos(8\theta_{eq})] + B_2[1-|\cos(2\theta_{eq})|] \quad (5)$$

In order to capture the local peak or dip that might occur when wind flow aligns with the diagonals of the ground surface of the courtyard, we perform a bi-linear mapping of the incidence flow angle θ onto θ_{eq}

$$\begin{cases} \theta_{eq} = 45^\circ \frac{\theta}{\theta_d} & 0^\circ \le \theta \le \theta_d \\ \theta_{eq} = 45^\circ \left(1 + \frac{\theta-\theta_d}{90^\circ-\theta_d}\right) & \theta_d < \theta \le 90^\circ \end{cases} \quad \text{with } \theta_d = \tan^{-1}\left(\frac{w}{\ell}\right) \quad (6)$$

where θ_d corresponds to the orientation of the diagonal. Fig. 11 illustrates the mapping procedure. The figure depicts the last term of Eq. (5), once plotted as a function of θ (top figure) and once as a function of θ_{eq} (bottom figure). The proposed mapping of θ onto θ_{eq} preserves the 0° and 90° orientations. θ_d is always mapped onto 45°, regardless the length-to-width ratio of the courtyard. For that orientation, the last term in Eq. (5) reaches a maximum. The peak hence always coincides with wind flow aligned with the diagonal of the ground surface of the courtyard.

The coefficients in Eq. (5) are assumed to depend solely on the geometrical characteristics of the courtyard. Inspired by the fact that the rate-of-change of the dimensionless exchange flux decreases with increasing length-to-height ratio, we propose an exponential relationship

$$A_{2n}\left(\frac{\ell}{h},\frac{w}{h}\right) = A_{2n,\infty} + (A_{2n,1}-A_{2n,\infty})\exp\left(-a_{2n}\left(\frac{\ell}{h}-\frac{w}{h}\right)\right) \quad (7a)$$

$$B_2\left(\frac{\ell}{h},\frac{w}{h}\right) = B_{2,\infty} + (B_{2,1}-B_{2,\infty})\exp\left(-b_2\left(\frac{\ell}{h}-\frac{w}{h}\right)\right) \quad (7b)$$

where A_{2n} equals $A_{2n,1}$ for a courtyard with ℓ/w equal to one, and tends asymptotically towards $A_{2n,\infty}$ for an urban street canyon ($\ell/w=\infty$). Similarly, B_2 equals $B_{2,1}$ for a courtyard with ℓ/w equal to one, and $B_{2,\infty}$ for an urban street canyon ($\ell/w=\infty$). The coefficients a_{2n} and b_2 define the rate-of-change of A_{2n} and B_2 with $(\ell-w)/h$, respectively. Remark that $w/h=1$ for all investigated courtyard configurations. The validity of the proposed parameterization for $w/h\neq 1$ still needs to be investigated.

If we want Eqs. (5–7) to be valid for a 1:1:1 courtyard ($\ell/w=1$), coefficients $A_{2,1}$ and $A_{6,1}$ should be zero. Indeed, these coefficients are the amplitudes of the harmonic contributions with a period of $360^\circ/(4n)$ with $n\neq 2m$. If they were non-zero, the equivalence of flow from e.g. 30° and 60° would not be guaranteed. Additionally, coefficient $B_{2,\infty}$ should vanish for an infinitely long street canyon, due to the absence of a diagonal. The parameters $A_{2n,1}$, $A_{2n,\infty}$, $B_{2,1}$, a_{2n} and b_2 can be freely chosen to capture the CFD data as closely as possible. They are determined by minimizing the error between the proposed parameterization (Eqs. (5–7)) and the RANS or LES CFD data. The resulting parameters are summarized in Table 1. $A_{6,1}$ and $A_{6,\infty}$ were found to be zero. Therefore, A_6 is always zero (Eq. (7a)) and the corresponding term can be omitted from Eq. (5).

In Fig. 12, the proposed parameterization is compared to the results from the CFD simulations. The coefficient of determination (R^2) is 80.4% for RANS and 90.0% for LES. Considering the fact that only 13 parameters are used in order to fit 32 CFD calculations, this result indicates the essential correctness of the proposed parameterization. Adding more terms to Eq. (5) will improve the quality of the fit, but requires the determination of additional parameters.

5. Ventilation potential

5.1. Definition

We define the ventilation potential (VP) as the weighted sum of the normalized exchange fluxes for every wind direction. The

Table 1
Parameters in Eqs. (5–7) as obtained by minimizing the error between the proposed parameterization (Eqs. (5–7)) and the RANS or LES CFD data.

N	RANS			LES		
	$A_{2n,1}$	$A_{2n,\infty}$	a_{2n}	$A_{2n,1}$	$A_{2n,\infty}$	a_{2n}
0	0.01172	0.052	0.222	0.00465	0.079	0.286
1	–	0.026	0.101	–	0.042	0.232
2	−0.00977	−0.039	0.161	−0.00162	−0.046	0.344
3	0.00034	0.017	0.177	0.00078	0.011	0.278
	$B_{2n,1}$	$B_{2n,\infty}$	b_{2n}	$B_{2n,1}$	$B_{2n,\infty}$	b_{2n}
1	−0.01653	–	0.765	−0.00250	–	19.927

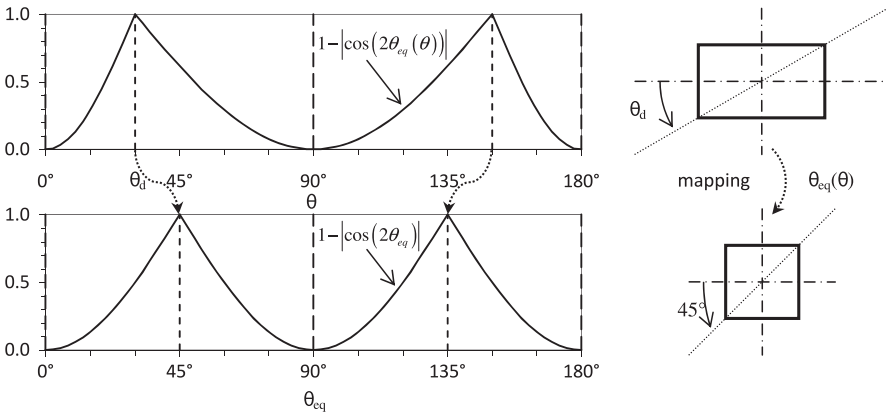

Fig. 11. Graphical illustration of the mapping of θ on θ_{eq} by means of Eq. (6).

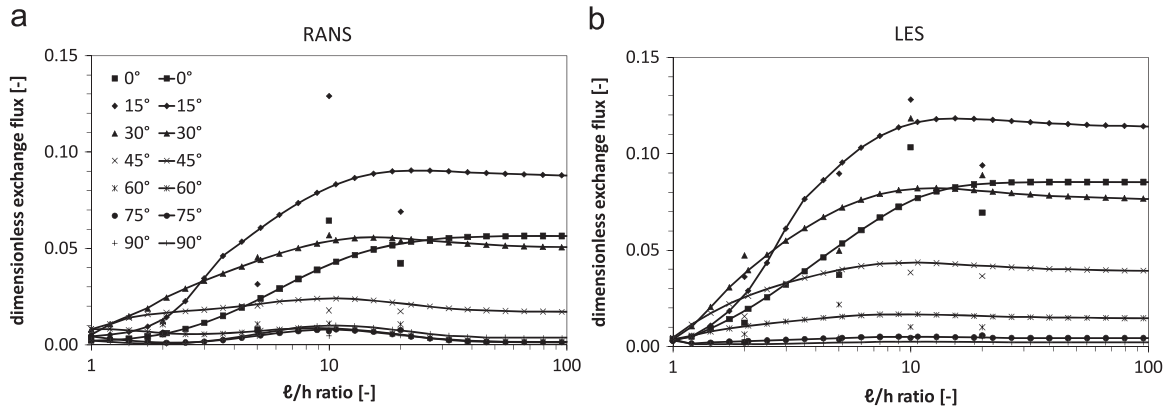

Fig. 12. Normalized exchange flux as a function of the ℓ/h ratio ($w/h=1$) based on (a) RANS and (b) LES data. Markers indicate simulated results, while solid lines with markers represent the corresponding parameterization according to Eqs. (5–7).

weighting factor is the product of the relative frequency P_θ of wind coming from direction θ and the corresponding time-averaged horizontal wind speed at 10 m height $U_{10,\theta}$

$$VP = \sum_\theta P_\theta U_{10,\theta} f_{\ell,\theta} \quad \text{with} \sum_\theta P_\theta = 1 \tag{8}$$

The VP is a statistical measure for the mean air flux exchanged between the courtyard or canyon and the urban boundary layer. Multiplied with the (average) difference in scalar concentration between the air entering and leaving the courtyard or canyon via the top surface, we obtain the net scalar removal (or accumulation) rate. The inverse relationship holds as well. Division of the known scalar production rate in the courtyard or canyon by the VP provides an estimate for the difference between the background concentration in the urban boundary layer and the average concentration in the courtyard or canyon.

The VP gives insight in the effect of local wind conditions, such as the distribution of wind speed and direction, on the exchange rate, and hence the air quality. Although the concept is general, the current simulations on which VP is based have certain limitations. For example, the effect of turbulence intensity has not been analyzed, nor was thermal stratification considered.

5.2. Application example

As an example, we compute the VP for a 1:1:2 courtyard exposed to the local wind conditions at Schiphol, the Netherlands. The frequency distribution (P_θ) of the local wind speed is shown in Fig. 13(a). As can be seen, the prevailing wind direction for Schiphol is south-west.

The exchange flux through the top-plane of the 1:1:2 courtyard is computed for a reference velocity $U_{10}=10$ m/s, based on the parameterization proposed in Section 4 and is illustrated in Fig. 13(b) as a function of the incidence flow direction. The parameterization based on the RANS calculations is represented with a dashed line, the one based on LES with a solid line. LES predicts significantly higher fluxes than RANS for incidence angles of 15° and 30°, moderately higher ones for 0° and 45° and lower ones for incidence angles between 60° and 90°. The peak at 30° is related to the fact that this wind direction aligns with a diagonal of the courtyard.

Since the frequency distribution of the local wind speed is only given in 30° intervals, the exchange fluxes are averaged over the same intervals. The averaged values are then used in Eq. (8) to compute the VP. Fig. 13(c) depicts the VP based on the RANS (dashed line) and LES (solid line) parameterization as a function of the courtyard orientation. The LES-VP is always about two times larger than the RANS-VP, demonstrating the importance to consider flow unsteadiness. The highest LES-VP is found for an SWW-NEE courtyard orientation, closely followed by a SSW-NNE orientation. For these two cases the prevailing SSW-SWW-wind enters at the optimal angle of 15–30°. A NNW-SSE courtyard-orientation, orthogonal to the prevailing wind direction, leads to the lowest VP.

6. Conclusions

We have conducted both steady (RANS) and unsteady (LES) simulations of the wind flow pattern in elongated courtyards. Both the courtyard length and the incidence angle were systematically varied.

The study reveals that the amount of exchange between the courtyard and the urban boundary layer is maximal when the angle between the incident flow and the principal courtyard axis is between 15° and 30°, regardless of the courtyard length. The 90°-case, commonly studied in literature, presents the lowest exchange rate. This is due to the presence of a standing vortex, almost fully uncoupled from the flow in the urban boundary layer. The minimum exchange rate proved to be independent of the courtyard length. For along-courtyard flow (0°), two different flow regimes could be identified based on the courtyards length-to-height ratio. For short courtyards, an isolated standing vortex is formed, while for more elongated courtyards the flow submerses at one end and surfaces at the other end.

The normalized exchange flux increases with increasing courtyard length, and is optimal for a length-to-width ratio of 10 or more. Longer courtyards can be considered as street canyons.

Simulations based on LES generally lead to higher exchange fluxes as compared to RANS. The largest differences were found for the 1:1:1 reference courtyard for the 0° and 30° wind directions. The differences between both simulation methods reduce with increasing courtyard length. The higher upward exchanges fluxes predicted by LES indicate the importance of unsteadiness on the exchange fluxes. Further experimental analysis is needed to validate these findings and give an answer on the accuracy of RANS and LES.

A parameterization was established that allowed extrapolating these results to the theoretical limit case of the (infinitely long) urban street canyon under oblique flow conditions. The parameterization can also be used to evaluate the normalized exchange flux for courtyards of different lengths and/or subjected to different incidence angles than the ones studied in this paper.

Based on the normalized exchange flux between the courtyard and the urban boundary layer, we have defined the ventilation

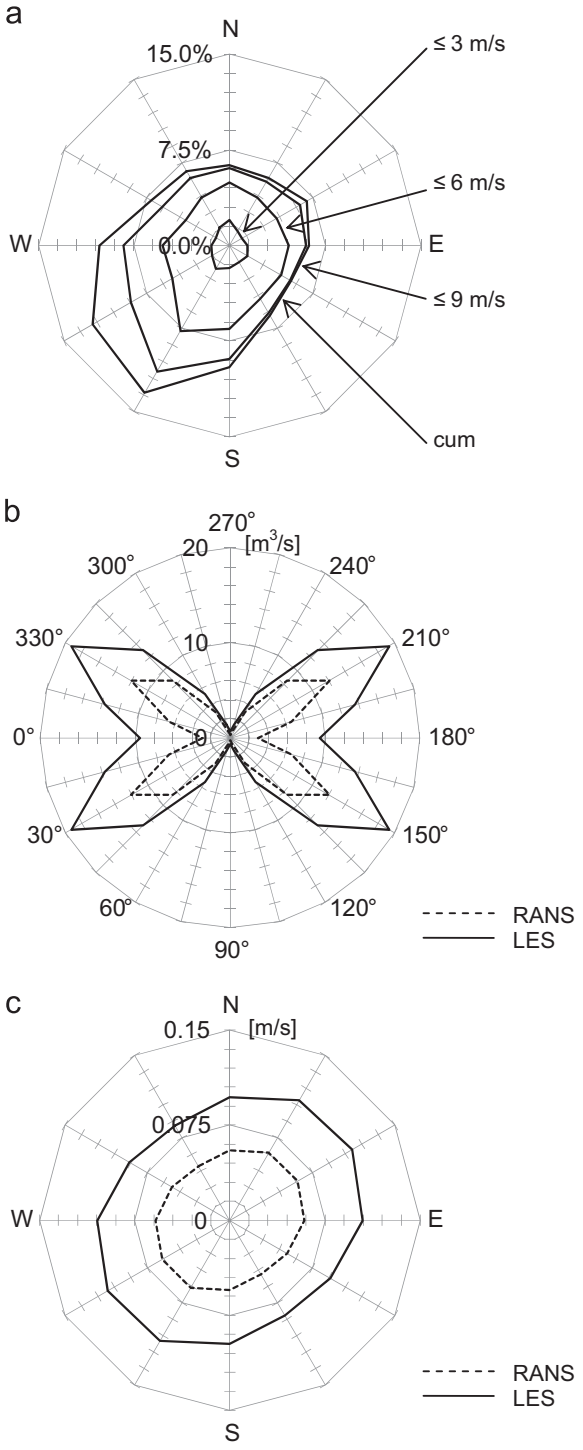

Fig. 13. (a) Wind rose for Schiphol, the Netherlands. Comparison between RANS (dashed) and LES (solid) of (b) the total exchange flux through the top-plane of a 1:1:2 courtyard as a function of the direction of the incidence wind flow for a reference velocity U_{10}=10 m/s, and (c) the corresponding VP as a function of the courtyard orientation.

potential (VP). The VP incorporates local wind data to assess the removal of scalars from, or the dilution of scalars within the courtyard or street canyon at a given geographic location. An illustrative example showed that the VP, in combination with the proposed parameterization, provides a useful tool to optimize the orientation and the dimensions of a courtyard, as function of the local wind data and the desired degree of removal. These conclusions can have a decisive impact on urban planning, human comfort and health.

References

Ansys Inc., Ansys Fluent 12.0 User's Guide, 2009.

Bady, M., Kato, S., Huang, H., 2008. Towards the application of indoor ventilation efficiency indices to evaluate the air quality of urban areas. Building and Environment 43, 1991–2004.

Baik, J.-J., Kim, J.-J., 2002. On the escape of pollutants from urban street canyons. Atmospheric Environment 36, 527–536.

Bartzis, J.G., Vlachogiannis, D., Sfetsos, A., 2004. Thematic area 5: Best practice advice for environmental flows. The QNET-CFD Network Newsletter 2 (4), q34–39.

Bechmann, A., 2006. Large-eddy simulation of atmospheric flow over complex terrain. Diss., DTU, Denmark.

Blocken, B., Stathopoulos, T., Carmeliet, J., 2007. CFD simulation of the atmospheric boundary layer—wall function problems. Atmospheric Environment 41, 238–252.

Buccolieri, R., Sandberg, M., Di Sabatino, S., 2010. City breathability and its link to pollutant concentration distribution within urban-like geometries. Atmospheric Environment 44, 1894–1903.

Cheng, W.C., Liu, C.-H., Leung, D.Y.C., 2008. Computational formulation for the evaluation of street canyon ventilation and pollutant removal performance. Atmospheric Environment 42, 9041–9051.

Franke, J., Hellsten, A., Schlünzen, H., Carissimo, B. (Eds.), 2007. COST Action.

Gromke, C., Ruck, B., 2009. On the impact of trees on dispersion processes of traffic emissions in street canyons. Boundary-Layer Meteorology 131, 19–34.

Hang, J., Sandberg, M., Li, Y., 2009. Age of air and air exchange efficiency in idealized city models. Building and Environment 44, 1714–1723.

Hargreaves, D.M., Wright, N.G., 2007. On the use of the k–ε model in commercial CFD software to model the neutral atmospheric boundary layer. Journal of Wind Engineering and Industrial Aerodynamics 95 (5), 355–369.

Johnson, G.T., Hunter, L.J., 1999. Some insights into typical urban canyons airflows. Atmospheric Environment 33, 3991–3999.

Kato, S., Huang, H., 2009. Ventilation efficiency of void space surrounded by buildings with wind blowing over built-up urban area. Journal of Wind Engineering and Industrial Aerodynamics 97, 358–367.

Kim, S.-E., Choudhury, D., 1995. A near-wall treatment using wall functions sensitized to pressure gradient. ASME FED 217, 273–280.

Kim, J.-J., Baik, J.-J., 2004. A numerical study of the effects of ambient wind direction on flow and dispersion in urban street canyons using the RNG k–ε turbulence model. Atmospheric Environment 38, 3039–3048.

Lilly, D.K., 1992. A proposed modification of the Germano subgrid—scale closure method. Physics of Fluids A 4, 633–635.

Liu, C.-H., Leung, D.Y.C., Barth, M.C., 2005. On the prediction of air and pollutant exchange rates in street canyons of different aspect ratios using large-eddy simulation. Atmospheric Environment 39, 1567–1574.

Martilli, A., Santiago, J.L., 2007. CFD simulation of airflow over a regular array of cubes. Part II: analysis of spatial average properties. Boundary-Layer Meteorology 122, 635–654.

Oke, T.R., 1988. Street design and urban canopy layer climate. Energy and Buildings 11, 103–113.

Pascheke, F., Barlow, J.F., Robins, A., 2008. Wind-tunnel modelling of dispersion from a scalar area source in urban-like roughness. Boundary-Layer Meteorology 126, 103–124.

Pavageau, M., Schatzmann, M., 1999. Wind tunnel measurements of concentration fluctuations in an urban street canyon. Atmospheric Environment 33, 3961–3971.

Richards, P.J., Hoxey, R.P., 1993. Appropriate boundary conditions for computational wind engineering models using the k–ε turbulence model. Journal of Wind Engineering and Industrial Aerodynamics 46–47, 145–153.

Ryu, Y.-H., Baik, J.-J., 2009. Flow and dispersion in an urban cubical cavity. Atmospheric Environment 43, 1721–1729.

Sagrado, A.P.G., Van Beeck, J., Rambaud, P., Olivari, D., 2002. Numerical and experimental modelling of pollutant dispersion in a street canyon. Journal of Wind Engineering and Industrial Aerodynamics 90, 321–339.

Sergent, E., 2002. Vers une méthodologie de couplage entre la simulation des grandes échelles et les modèles statistiques. PhD thesis, École centrale de Lyon, Lyon, France.

Shih, T.-H., Liou, W.W., Shabbir, A., Yang, Z., Zhu, J., 1995. A new k–ε eddy viscosity model for high Reynolds number turbulent flows. Computers & Fluids 24, 227–238.

Sini, J.-F., Anquetin, S., Mestayer, P.G., 1996. Pollutant dispersion and thermal effects in urban street canyons. Atmospheric Environment 30, 2659–2677.

Soulhac, L., Garbero, V., Salizzoni, P., Mejean, P., Perkins, R.J., 2009. Flow and dispersion in street intersections. Atmospheric Environment 43, 2981–2996.

Tominaga, Y., Mochida, A., Shirasawa, T., Yoshie, R., Kataoka, H., Harimot, K., Nozu, T., 2004. Cross comparisons of CFD results of wind environment at pedestrian level around a high-rise building and within a building complex. Journal of Asian Architecture and Building Engineering 3, 63–70.

Vandoormaal, P., Raithby, G.D., 1984. Enhancements of the SIMPLE method for predicting incompressible fluid flows. Numerical Heat Transfer 7, 147–163.

Van Leer, B., 1979. Towards the ultimate conservative difference scheme. V - A second-order sequel to Godunov's method. Journal of Computational Physics 32, 101–136.